Ore Geology Reviews 139 (2021) 104581

Contents lists available at ScienceDirect

Ore Geology Reviews

journal homepage: www.elsevier.com/locate/oregeorev

Geophysical characterisation of geologic features with mining implications from ERT, TDEM and seismic reflection (Mining District of Linares-La Carolina, Spain)

R. Mendoza [a], J. Rey [b,*], J. Martínez [a], M.C. Hidalgo [b], S. Sandoval [c]

[a] Dpto. de Ingeniería Mecánica y Minera, EPS de Linares and CEACTEMA, Universidad de Jaén, Campus Científico Tecnológico, 23700 Linares, Jaén, Spain
[b] Dpto. de Geología, EPS de Linares and CEACTEMA, Universidad de Jaén, Campus Científico Tecnológico, 23700 Linares, Jaén, Spain
[c] Everest Geophysics Consulting, 28270 Colmenarejo-Madrid, Spain

ARTICLE INFO

Keywords:
Faults
Seismic reflection
Electrical resistivity tomography
Time-domain electromagnetic
Linares-La Carolina mining district
Spain

ABSTRACT

In this study, the effectiveness of different geophysical techniques is analysed in relation to the imaging of geological structures with mining interest. To achieve this goal, the old district of Linares-La Carolina (Southeast Spain) is chosen due to the presence of dense swarm of mineralised dykes, primarily consisting of galena (PbS). In particular, the western boundary of the mining district is studied. At this westernmost area the veins lose their continuity due to regional fractures which resulted in the abandoning of the extracting labours.

Direct information from both the surface geology and several boreholes are used as ground-truth calibration and verification for the geophysical tools used in this study.

The seismic response is characterised by high-amplitude reflectors, generally at the base of the sedimentary cover. The seismic profiles suggest lateral changes in the thickness and the existence of fractures affecting the sedimentary cover and/or the top of the acoustic basement. However, this technique has proved ineffective when studying the Palaeozoic substrate, precisely at those areas where the veins are hosted.

Electrical resistivity tomography (ERT) studies suggest fractures and lateral changes in the facies, in both the sedimentary cover and the Palaeozoic basement. The basement shows phyllites in the granite intrusion, which are crucial for the elastic properties of the hosting rock and therefore indicate areas prone to further mineralisation. Time-domain electromagnetic (TDEM) data, which is an excellent complement to the two previous techniques, have also been collected. Data have been taken with different configurations and varying measurement parameters at each sounding station. This approach has made it possible to compare the effectiveness benefits and drawbacks of the different methods.

1. Introduction

Geophysical prospecting techniques and their application to studying mining basins have evolved considerably in recent years. The emergence of automatic data acquisition systems, the availability of powerful computers, and the development of two- and three-dimensional numerical modelling methods have markedly enhanced the resolutions of complex geological models (Loke and Barker, 1996; André et al., 2012; Binley et al., 2015).

Among the advantages associated with these techniques are their relatively low cost, the possibility of covering large survey areas, the vast amount of data they provide, and their non-destructive nature. Among their drawbacks, we must note the non-uniqueness of the results because they are indirect techniques requiring a data inversion process. Another disadvantage is the decrease of resolution with depth (Telford et al., 1990). For these reasons, a good practice in geophysics consists of using at least two different methods to reduce the indeterminacy (André et al., 2012; Granda Sanz et al., 2019; Martínez et al., 2016; Martínez et al., 2019; Rey et al., 2020; Rey et al., 2021).

Geophysical methods applicable to geological-mining research are numerous and varied, including gravimetric, magnetic, electrical, electromagnetic, and seismic methods. All of them can contribute to the ore deposit exploration in some way.

This study aims to analyse the capacity of electrical (electrical resistivity tomography, ERT), electromagnetic (time-domain electromagnetic surveys, TDEM) and seismic (seismic reflection) techniques when

* Corresponding author.
E-mail address: jrey@ujaen.es (J. Rey).

https://doi.org/10.1016/j.oregeorev.2021.104581
Received 8 September 2021; Received in revised form 7 November 2021; Accepted 9 November 2021
Available online 15 November 2021

studying geological structures with mining implications. For this purpose, the old mining district of Linares-La Carolina (Southeast Spain, Fig. 1A) has been chosen. In addition to detailed geological surface data, direct data on numerous boreholes (Fig. 1B) and seismic lines in this mining district are available. Combined, this information provides verification and correlation tools (ground-truth data) for the indirect techniques used in this research.

This mining district contains mineralised dykes, primarily consisting of galena (PbS), hosted in Palaeozoic granitoids (Azcárate, 1977; Lillo 1992; Larrea et al., 1994). The sector was subjected to intense mining and subsequently abandoned in the 1970s. The mines were then closed due to the drop in the price of this mineral and the depletion of reserves.

2. Geological setting

In the study region, two geological units can be differentiated: the

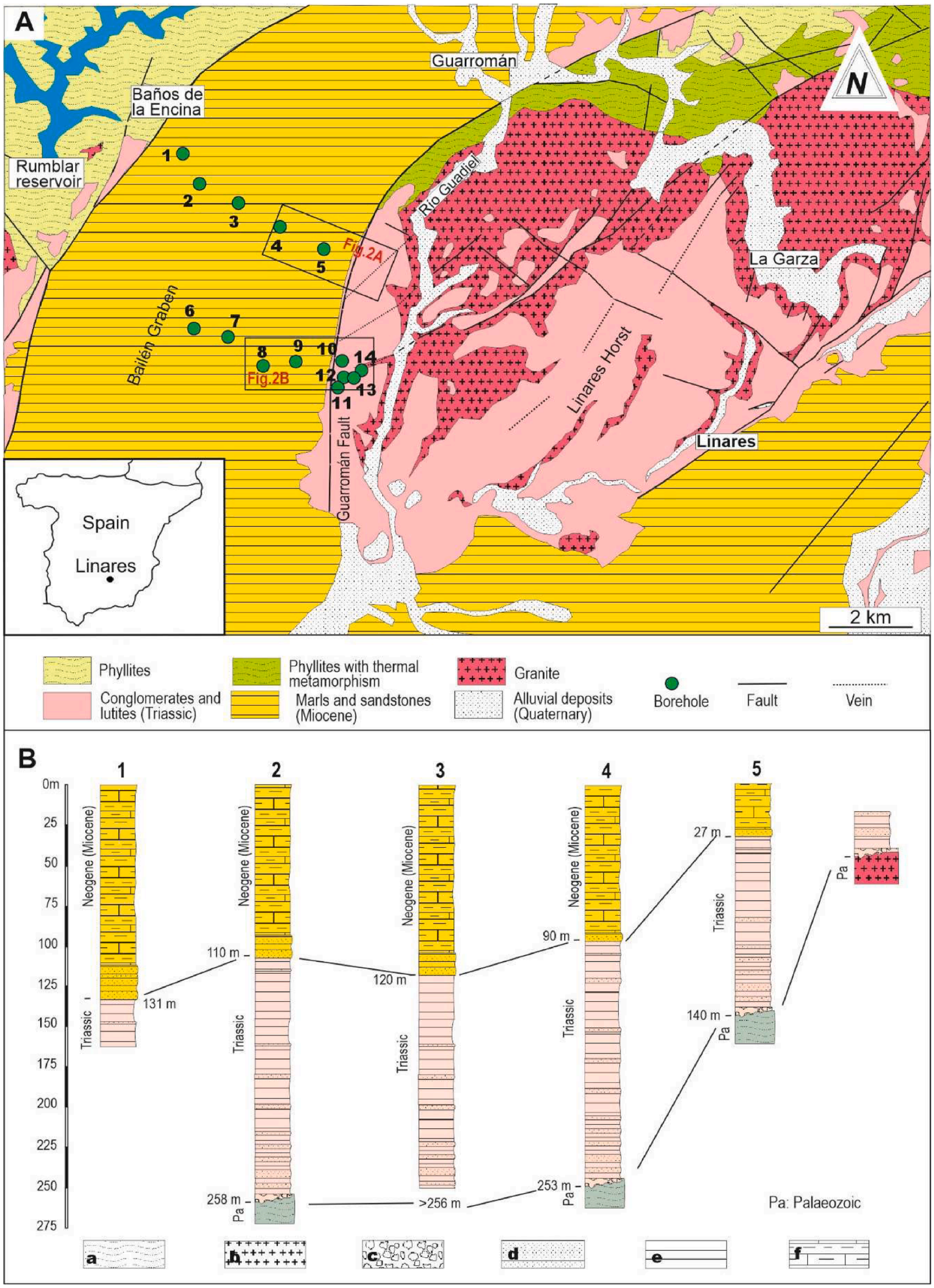

Fig. 1. (A) Regional geological map, showing the location of the two sectors studied and mapped in Fig. 2A and 2B, as well as the position of different mining research boreholes. (B) Stratigraphic columns based on data from mining research boreholes. a. - phyllites, b. - granitoids, c. - conglomerates, d. - sandstones, e. - clays, f. - marl and marly limestones.

Palaeozoic Basement and the Tabular Cover of the Iberian Plateau (also known as Meseta). The former primarily consists of intensely folded phyllites intruded by a granite stock in the last stages of the Hercynian Orogeny (Azcárate, 1977; Larrea et al., 1994). This intrusion produces a widespread contact metamorphism aureole with a highly variable width and outcrops in the mining district, predominantly with a horst structure (Fig. 1A). Discordantly overlying this basement and arranged subhorizontally, the post-Hercynian sedimentary cover is composed of Triassic, Miocene, and Quaternary materials (Fig. 1A and B). The Triassic cover mainly consists of red shale, with thicknesses approximately ranging from 50 to 100 m, and contains a 10- to 20-m-thick basal conglomerate layer in which sandstone beds alternate with shale facies. The Miocene materials are deposited on this suite and separated via a stratigraphic discontinuity. At the base, a calcarenite breccia bed changes laterally and vertically to marls and marly limestones with thin calcarenite intercalations. The Quaternary cover contains silt, sand and gravel and is only associated with the sedimentary filling of riverbeds (Azcárate, 1977; Rey et al., 2013a; Martínez et al., 2016; Martínez et al., 2019).

The origin of the mineralised dykes in this mining district is associated with extensional conditions and an anomalous geothermal gradient that originated at the end of the Hercynian Orogeny. The hydrothermal mineralisations resulted from the injection of the fluid phase and metals through old fractures N35-N60E and NS-N20E in the Palaeozoic basement and in the granite body. These hydrothermal veins mainly consist of galena, sphalerite, chalcopyrite, pyrite, quartz, ankerite and calcite (Azcárate, 1977; Lillo, 1992).

Lithological control is essential in mineralisation: the veins metallise when they are hosted in the granite stock, while quickly turning into waste rock when they do so in phyllites. On one hand, mechanical factors account for this process because competent materials (granitoids) allow a frank and sharp fracturing, while incompetent materials (phyllites) react to the stress by deforming, thus hampering the formation of open spaces. On the other hand, within the metamorphic aureole created by granite in the western sector (Fig. 1A), the phyllites allow metallised veins, which are lost or disappear when hosted outside this aureole. The

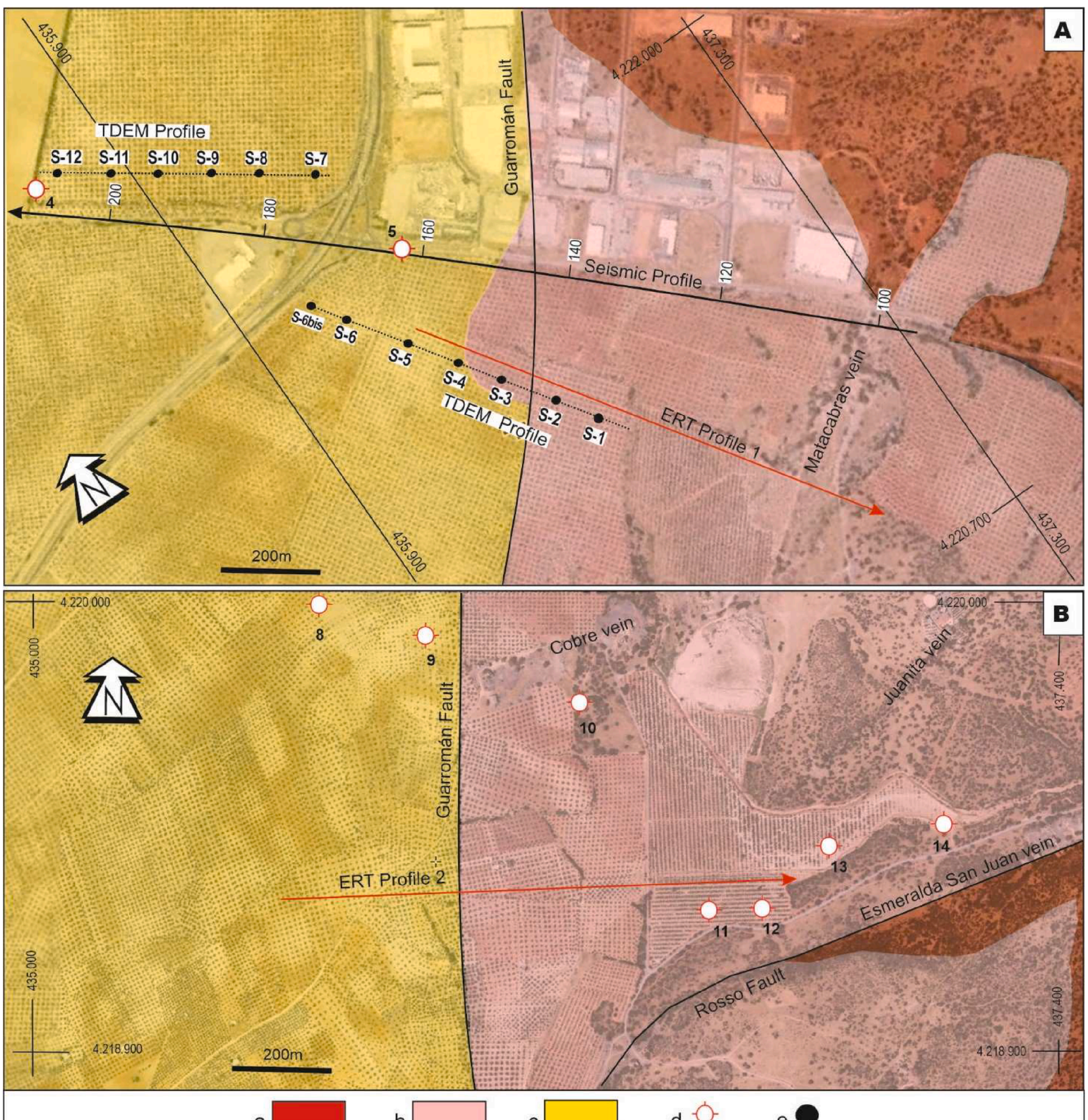

Fig. 2. Details of the two study sectors (A and B) whose locations are shown in Fig. 1A, highlighting the position of the different TDEM stations (S1, S2, S3, S4, S5, S6, S6bis, S7, S8, S9, S10, S11 and S12), the seismic profile, the ERT profiles and the location of the boreholes (4, 5, 8, 9, 10, 11, 12, 13 and 14), whose characteristics are outlined in Table 1. a. - granitoid, b. - Triassic clays and sandstones, c. - Miocene marls and marly limestones, d. - borehole, e. - TDEM station.

veins are lost because these materials undergo physical changes resulting from a contact metamorphism, thereby becoming more competent.

On the western boundary of the mining district, technical reports (ENADIMSA, unpublished results) indicate the presence of a structure (known as AA), with an approximately NS direction and associated with a fault breccia with ankerite and some galena. This structure was developed prior to the deposit of Triassic materials, causing the collapse of hundreds of metres of granite stock and phyllites with thermal metamorphism in the western sector (Bailén Graben). For this reason, this structure brings facies of varying competence into contact, which is crucial for the development of mining operations. Its location will make it possible to outline the areas of greatest interest for mining research.

This structure and other subparallel structures have been reactivated in post-Palaeozoic stages. The last manifestation of these movements gave rise to the surface-mappable Guarromán Fault (Fig. 1A, Fig. 2A and B), which defines the western boundary of the mining district. This study aims to characterise these structures by combining the aforementioned geophysical techniques.

3. Materials and methods

3.1. Seismic reflection method

Seismic reflection profiles collected in the 1980s by the Geological and Mining Institute of Spain (*Instituto Geológico y Minero de España* – IGME, unpublished results) have been analysed. The Mini-Sozie method was applied, and SM-7GR geophones with a 30-Hz sensor were used to record the resulting signals.

The geophones were arranged in groups arrays of 18 units per trace. At each recording station the geophones were laid 1.85 m apart. The distance between traces was 15 m.

At each source point an average of 2,100 pulses were generated. Seismic reflection tests were performed with source offsets of 30, 45, 60 and 75 m, identifying the best reflections at a distance of 45 m. The data were processed by *Compagnie Générale de Géophysique* (CGG). The processing flow followed a standard processing sequence, including point collection along a "Slalom line", prestack deconvolution, static corrections, continuous velocity analysis, dynamic velocity corrections, automatic adjustment of residual static corrections, addition, filter (30 Hz in low and Notch), coherence improvement, and migration (IGME, unpublished results).

This study focuses on one of the seismic lines, namely on line 1 (its location is shown in Fig. 1A and in Fig. 2A). For the two-way-traveltime/depth transformation, average velocities up to the base of the Miocene of about 1,900 m/s are estimated (IGME, 1983) which would correspond to traveltimes up to 100–150 ms. For the Triassic, with times up to 190–240 ms, the estimated velocities are about 2200 m/s.

This is the velocity that is marked when processing the seismic line and that has been verified by measuring the thickness of different units in the existing boreholes (Fig. 1B and Table 1).

3.2. Electrical resistivity tomography (ERT) method

This geophysical prospecting technique consists of measuring the apparent resistivity distribution in the subsoil from a very high number of observations made from the ground surface (Telford et al., 1990; Store et al., 2000). Differences in the geoelectric behaviour are expressed as 2D profiles, which are one of the most effective nondestructive tools for studying and characterising subsoil discontinuities (Sasaki, 1992; Store et al., 2000). In recent years, this technique has been widely used with satisfactory results in stratigraphic (Maillet et al., 2005; Martínez et al., 2009; Rey et al., 2013a), hydrogeological (Goldman et al., 1994; Auken et al., 2003; Martínez et al., 2009; André et al., 2012) and environmental studies (Martínez et al., 2016; Martínez-Pagán et al., 2009; Rey et al., 2013b; Rey et al., 2021; Martínez-Segura et al., 2020).

In the mining district of Linares, the (very conductive) galena veins are embedded in the (very resistive) host granitic bedrock. The different electrical behavior between both lithologies makes their detection with geoelectrical surveying methods very favorable. In this regard, previous investigations in nearby locations show very promising results (Martínez et al., 2019). However, most of the times the small size of the ore veins requires using high-density inter-electrode spacings which results in a reduced depth of investigation. For this reason, in previous works the investigated sites were selected for their thin sedimentary cover where the host granite and the embedded veins were at depths between 20 and 40 m. In this study, the sedimentary cover is thicker, and the main goal is to distinguish the consolidated bedrock with the capacity to host ore veins (granite) from that one where the development of ore veins is more difficult (phillites). A large inter-electrode spacing (10 m in this study) allows a deeper investigation albeit with a reduced resolution.

The tomography method consists of implanting numerous metal electrodes in the ground along rectilinear profiles, with some separation between the electrodes depending on the degree of the target resolution and depth. Higher resolution require shorter separations between electrodes whareas greater investigation depth need longer electrode spacings (Sasaki, 1992). A Wenner-Schlumberger electrode configuration was used in this study. This configuration performs well and remains stable under both vertical and horizontal resistivity changes (Dahlin and Zhou, 2004; Loke, 2014), and is therefore highly useful when studying horizontal or slightly inclined beds, which may show lateral changes in facies and/or vertical structures, as is the case.

The electrodes are connected to a measuring device, which automatically controls the arrangement, selection and activation of the electrodes for each individual measurement following a preprogrammed sequence. At each observation point, the voltage and intensity are measured to calculate the apparent resistivity of the ground, which is attributed to a specific geometric point in the subsoil.

A RESECS resistivity-meter from *Deutsche Montan Technologie* (DMT) was used. The electrical resistivity tomography profiles have been interpreted based on the apparent resistivities obtained in the field work, treated using the specific program RES2DINV (Loke and Barker, 1996). This calculation program is based on the least squares method with a forced smoothing and modified with the Quasi-Newton optimisation technique. The inversion method builds a subsoil model using rectangular prisms and determines the resistivity values of each prism, minimising the differences between the observed and calculated apparent resistivity values (Loke and Barker, 1996; Loke and Dahlin, 2002).

In this study, two electrical resistivity tomography profiles have been collected in the NW-SE and W-E directions, with lengths of 1,110 m each, 112 electrodes and a spacing of 10 m between electrodes (Fig. 2).

Table 1
Depth of the contacts (expressed in m) between different geological units based on data from mining research boreholes. Their positions are shown in Fig. 1A. M. - Miocene, T. - Triassic, Pz. - Palaeozoic, Gr. - Granitoids, ph. – Phyllites.

Borehole	M-T contact depth (m)	T-Pz contact depth (m)	Ph-Gr contact depth (m)	Triassic thickness (m)
1	131	–		
2	110	258-Ph		148
3	120	>250		>130
4	98	253-Ph		155
5	27	140-Ph		113
6	141	252-Ph		111
7	66	194-Ph		128
8	27	163-Ph		136
9	20	181-Ph		161
10	–	48-Ph	273	–
11	–	55-Ph		–
12	–	60-Ph		–
13	–	77-Gr	–	–
14	–	30-Gr	–	–

3.3. Time-domain electromagnetic method (TDEM)

The operating principle of the time-domain electromagnetic method (TDEM) consists of circulating an electric current through a transmitter coil for short periods. When the current flow is abruptly interrupted, the primary magnetic field varies, which induces a variable electric current. This variation, in turn, generates a transient secondary magnetic field. These currents flow in closed paths and migrate in depth, decreasing in intensity over time. Changes in the secondary magnetic field over time induce a transient voltage in the receiving coil. The way in which this voltage decreases provides information on the conductivity distribution in the subsoil, which can then be used for its characterisation (Nabighian, 1988; Telford et al., 1990; McNeill, 1994).

The TDEM method has been typically used in field prospecting (Gómez-Ortiz et al., 2014; Xue et al., 2012; Granda Sanz et al., 2019), in hydrogeological studies (Fitterman and Steward, 1986; Danielsen et al., 2003) and in the analysis of sedimentary basins (Dennis and Cull, 2012; Sridhar et al., 2017; Rey et al., 2020). In recent times, this methodology has also been used in environmental studies (Hallbauer-Zadorozhnaya and Stettler, 2009; Hu et al., 2016) and in the characterisation of marine intrusions (Kafria and Goldman, 2006; Levi et al., 2008).

The TDEM measuring system used in this study was an AIE-2 model ELGEO Research & Production Company. This device has a maximum output power of 200 W and a current intensity of up to 10 A. The TDEM receiver is based on a 16-bit analogue–digital converter with a signal processor that provides noise-immune analogue–digital conversion of the input voltage and real-time signal preprocessing, and offers measurements ranging from 5 μs to 10 s, with an input voltage of 5–20 V with a signal compensation.

In the field campaign, a total of 13 TDEM measurement stations were installed in the SE-NW direction along the seismic line under study. The points located in Fig. 2A refer to the centre of the measurement stations at 100 by 200 m square loops. At each point, measurements have been taken using central- and single-loop configurations and varying the measurement parameters (intensity, time, and voltage), which makes it possible to compare the efficiency of different configurations. Thus, to reach study depths of approximately 100–200 m (the first stations), 100X100 m transmission loops have been used. In the last stations, given the greater depth of the Palaeozoic basement (more than 250 m), the measurements had to be repeated by increasing the dimensions of the transmitter loops (200X200 m) and using a wire with a section of 6 mm^2 gauge, which decreases its resistance and therefore makes it possible to reach a higher effective current intensity. When working with a central-loop configuration, the receiving coil had dimensions of 20X20 m with a 5-turn wire and a X10 amplifier. The software TEMBIN is used to visualise and edit the different curves. The modelling and inversion process is performed using the programs ZondTEM1D and ZondTEM2D.

4. Results and discussion

4.1. Seismic reflection method

In the study region, the sedimentary filling at the top of the seismic profiles provides a moderate reflector amplitude, which is interpreted as sandstones and marls of the Upper Miocene. This suite appears to be subhorizontal, with an overlapping morphology on the lower unit (see the interval between the seismic traces 260 and 220 in the seismic profile of Fig. 3), which matches the marine transgression that occurred in the region during the Upper Messinian (Perconing, 1971). A slight unconformity is associated with the stratigraphic discontinuity that separates the two units of the sedimentary cover. Under the Miocene materials, in the Triassic unit, beds of greater amplitude are also detected, which correlate with the powerful sandstone beds at the base of the Triassic unit observed both in the mechanical soundings and in outcrops. Laterally, the reflector at the base of the Triassic unit can be lost due to the changes in thickness, or even to the truncation of basal conglomerates, as noted in outcrops of the western sector of the Guarromán Fault. The Triassic Unit dips slightly to the NW (towards the centre of the Bailén Graben). The acoustic basement is formed by the Palaeozoic basement, which is characterised by chaotic features and disorganised seismic facies (Fig. 3). In the basement, the phyllites and the granite intrusion cannot be differentiated based on the seismic profile.

Different criteria, which in general have agreed well, have been used for the time-to-depth transformation. On one hand, geological field data have been used, specifically the thicknesses of the different units measured in the vicinity. On the other hand, the velocity values were also used, which are included in the profiles. Lastly, direct data were collected in the region, thanks to mining research (Fig. 3) and groundwater boreholes.

The seismic reflection profile shows a series of fractures affecting the basement and the sedimentary cover. The "AA Fault", which is barely detected because this fault does not affect the sedimentary cover, may be located in the easternmost sector of the profile. The Guarromán Fault is identified to the NW of the seismic profile (Fig. 3), which affects Miocene materials, according to outcrop data. To the south, this structure can reach up to 70 m in vertical throw, according to field observations. To the NW of the aforementioned fault, the profile shows

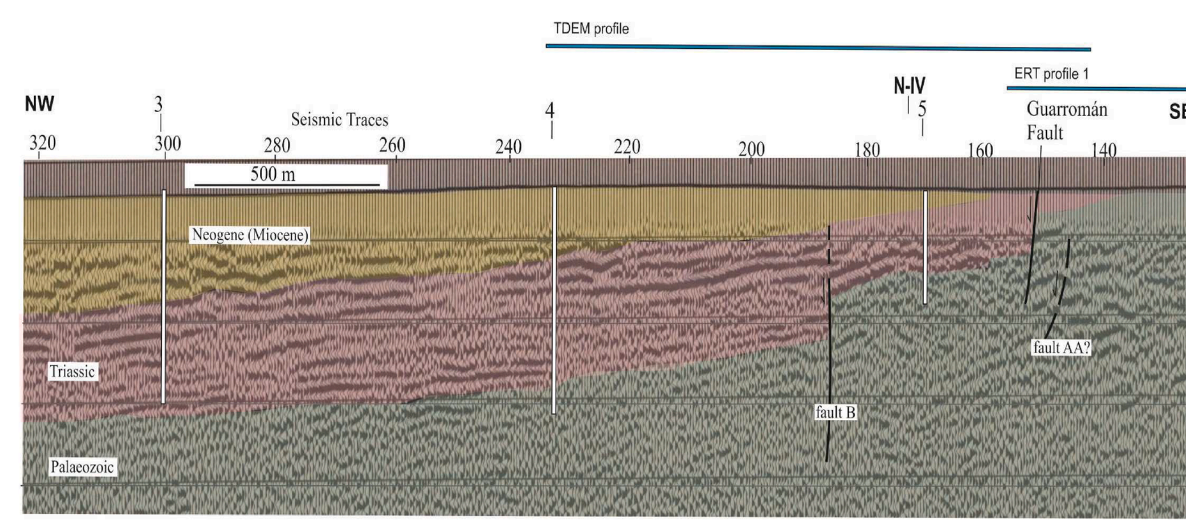

Fig. 3. Seismic reflection profile and interpretation (see location in Fig. 2A). The positions of the boreholes and the TDEM + ERT profiles are indicated. CDP common depth point.

"Fracture B", with a vertical throw of approximately 70 m, which affects the basement and part of the Triassic series (see Fig. 3). However, according to outcrop data, this fracture seems to be fossilised by the Miocene materials. Therefore, these three fractures have acted in different stages, albeit ultimately causing the subsidence of a graben to the NW (Bailén Graben) and the Linares horst.

4.2. Electrical resistivity tomography method

The electrical resistivity tomography profile 1 overlaps the SE end of the seismic profile (Fig. 2A), precisely where seismic exploration, given its shallow depth, does not provide a good visualisation of the contact between the sedimentary cover and the Palaeozoic basement (Fig. 3). The current injection time is 256 ms, with 128-ms delay. In total, 2,377 measurements were taken, with a final RMS fitting error of 5.8% reached in the 5th iteration of the inversion process. Fig. 4A shows ERT profile 1, which reaches a 220 m depth in the zone of maximum penetration. Based on the geoelectrical characteristics, two suites are differentiated: the first suite is characterised by its high resistivity values (between 100 and 3000 Ωm), which are associated with the Palaeozoic basement. These facies almost reach the surface in the SE end of the profile (Linares horst). In turn, in this suite electrical facies can differentiate granitic facies from phyllites, because granitoids provide much higher resistivities. This interpretation is confirmed thanks to mechanical mining research and groundwater boreholes in the sector. The ERT 1 profile suggests an abrupt subsidence of the granite towards the NW, as observed in the outcrop (in the NE sector of Fig. 1A). This subsidence could be associated with the structure that sank the NW block of the Hercynian age (without affecting the sedimentary cover), regionally detected in some mining operations and named the AA Fault (technical reports without publication). This regional structure would have great mining importance because it causes the subsidence of competent rocks (granitoid and metamorphic aureole) for several hundred metres. Accordingly, the phylonian structures, if any, would be located at much greater depths, reducing the probability of finding mineralised structures with sufficient entity to justify the exploitation.

On the Palaeozoic basement, a low-resistivity unit is associated with the sedimentary cover. This upper unit has a thickness of approximately 20–30 m throughout most of the profile. The resistivity and thickness increase sharply, but only in the NW sector, which is associated with the downward displaced block of the Guarromán Fault (Fig. 4A). In ERT profile 1, the Palaeozoic basement is not detected in the downward block of this fault; however, thanks to data from the nearby mechanical mining research boreholes (borehole 5), it is known to be 140 m deep (Fig. 4A).

. The injection time in the ERT profile 2 is 256 ms, with a delay of 128 ms. In total, 2,565 measurements were taken. The final model has a RMS error of 13% reached in the 4th iteration. The geological structure deduced from ERT Profile 2 (Fig. 4B), and confirmed thanks to the different boreholes, is equivalent to that measured in ERT 1 profile. Thus, borehole 12 intersects the upper section of the Triassic facies, under which phyllites appear to be affected by an intense contact metamorphism, given the proximity to granite (the granite has been drilled in boreholes 13 and 14). ERT profile 2 also shows the abrupt sinking of the granite towards the NW, most likely caused by the "AA Fault". Borehole 10 (Fig. 4B), located in a downward block according to this model, crosses a thick sequence of phyllites without any evidence of thermal metamorphism, up to 273 m of depth, where cuts a mineralised breccia associated with the "AA Fault", and subsequently granite from the footwall block (ENADIMSA, unpublished technical reports). ERT 2 profile also shows the Guarromán Fault (Fig. 4B). Boreholes 8 and 9, in the downward displaced block of this second structure, intersect the phyllites of the Palaeozoic basement at 163 and 181 m, respectively.

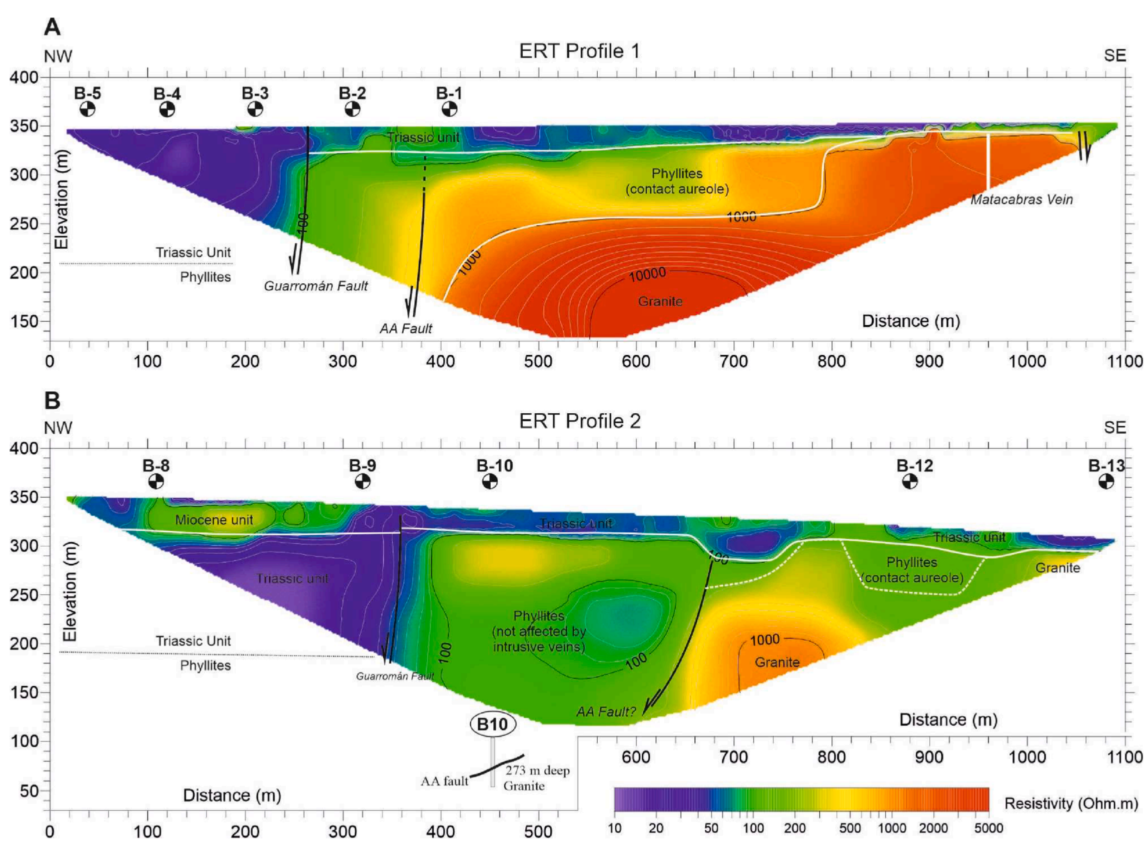

Fig. 4. Electrical resistivity tomography (ERT) profiles.

4.3. Time-domain electromagnetic method

In each measurement station, the TDEM profile has been measured by varying the size (100 m × 100 m or 200 m × 200 m) and the configuration (single or centred) parameters of the loops, injection amperage, voltage and measurements. In each test, the ramp time is directly proportional to the size of the loop and the amperage (Christiansen et al., 2009). In this study, according to technical specifications of the equipment, the ramp time was 7 or 15 μs, depending on whether the injected amperage was 1 or 8 A (for 100 m × 100-m loops) or 12 μs or 30 μs (for 200 m × 200 m loops).

The first campaign was performed with a 100 m × 100 m loop. This configuration makes it is possible to detect the contact between the Palaeozoic substrate and the sedimentary cover in the eastern sector (from station S1 to station S6bis, in Fig. 2A). For example, Fig. 5 shows the curves generated in stations S2 and S6bis (Fig. 5A and Fig. 5B, respectively), plotting the induced voltage (blue line) and apparent resistivity (red line) as a function of time, as well as the resistivity model generated by the inversion software (thick red line). All curves show the fit between the field curve and the curve of the ZONDTEM1D software model. In both cases, the goodness of the curve fit stands out, with RMS errors of 1.0% and 1.4% (S2 and S6bis, respectively).

The curve of station S2 highlights an increase in the resistivity at a depth of approximately 35 m, which is correlated with the contact between the Triassic facies (sandstones and clays) and the Palaeozoic phyllites (Fig. 5A). The resistivity gradually increases, which could be due to the presence of intensely altered phyllites in the top of the Palaeozoic basement (in line with observations in the outcrops and in boreholes of the sector).

The curves resulting from the data collected in stations S3 to S6bis are very similar to one another and differ from those obtained in the previous stations (stations S1 and S2) due to the increase in the depth at which the higher resistivity associated with the basement is detected. Thus, in station S6bis (Fig. 5B), the contact between the sedimentary cover (Miocene + Triassic) and the Palaeozoic basement (phyllites) is estimated at approximately 140 m. This interpretation is consistent with the data provided by existing boreholes (5 in Fig. 1B and Table 1) or seismic profiles (Fig. 3). Therefore, the comparison of the different stations makes it possible to locate the Guarromán fault using this geophysical prospecting method.

The depth at which the basement is located in the eastern sector makes it necessary to repeat the electromagnetic prospecting campaign with a 200 m × 200 m loop. For example, Fig. 5 shows the curves generated at station S10 (Fig. 5C). In this case, the goodness of the curve fit also stands out, with an RMS error of 1.3%. In the curve, an increase in the resistivity is detected from 250 m, which is associated with the contact between the Triassic sandstones and clays and the phyllites of the Palaeozoic basement. This depth correlates with that detected in borehole 4 (Fig. 1B, Fig. 2A and Table 1). The depths assessed in curves S7/S8/S9/S10/S11 and S12 are very similar. Therefore, comparing different stations makes it possible to detect an unmapped fracture, with approximately 90 m of throw, between stations S6bis and S7.

Fig. 5D shows the 2D section of resistivity obtained using the electromagnetic method, resulting from the combined inversion of the curves from thirteen individual stations using the ZondTEM2D software. In the SE sector, the Triassic unit (predominantly sandstone beds) and Palaeozoic phyllites have high resistivity values. The alteration of the top of the phyllites, as well as the associated decrease in resistivity, would allow for a weak differentiation between the two suites. Towards the NW, using this software the two fractures mentioned above are

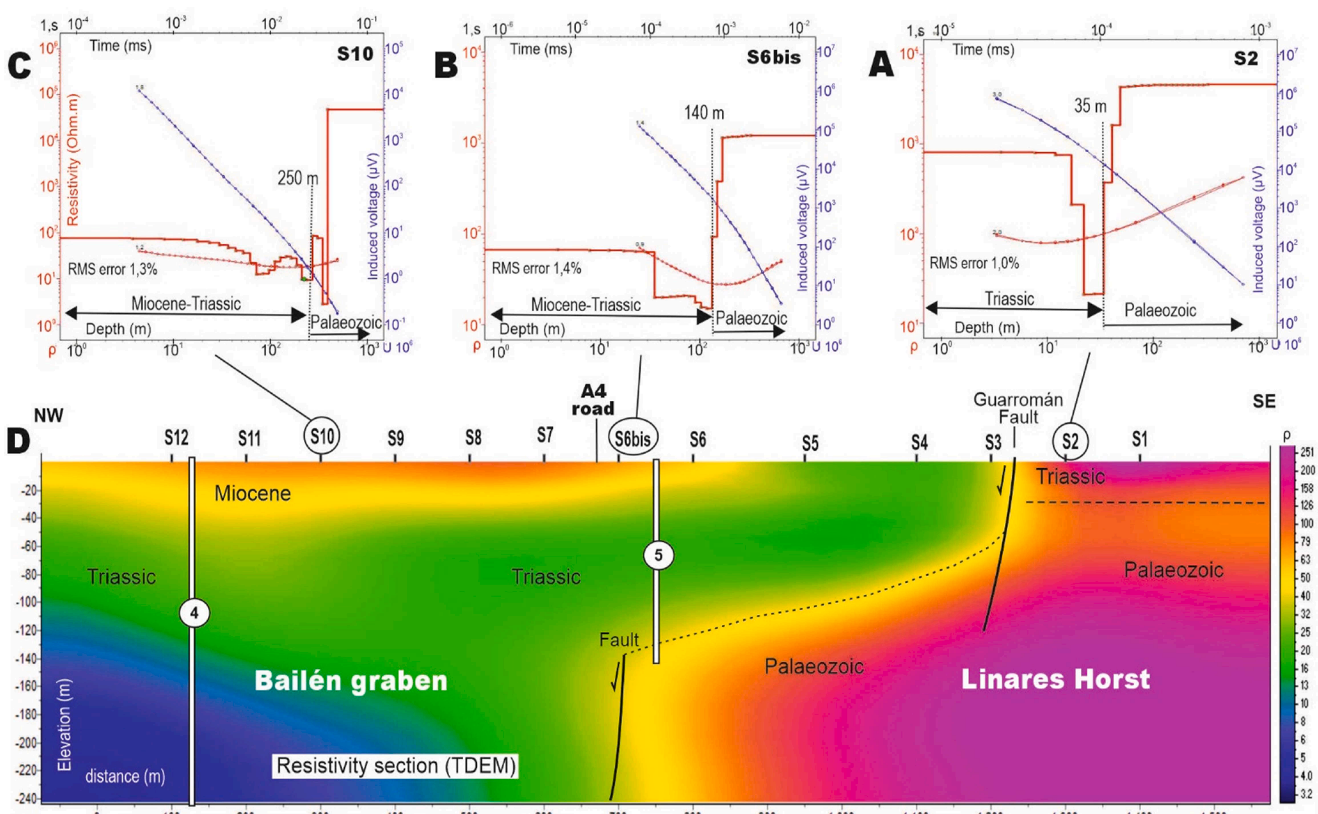

Fig. 5. Top: Induced voltage curves (blue line) and apparent resistivity (red line) as a function of time. For each of them, the fit between the field and the model (by the ZONDTEM1D software) lines is indicated. The interpretation after the inversion of the data is also included; red straight lines represent the resistivity as a function of the depth. In charts A, B and C, data collected at station S2, S6bis and S10 (Fig. 5A, 5B and 5C). Bottom: 2D resistivity model derived from the data inversion implemented in the program ZondTEM2D (Fig. 5D).

clearly detected and correlated with those identified in the seismic profile (Fig. 3). In turn, in the Bailén Graben differences in the electrical behaviour between the Miocene unit and the Triassic top allow us to indicate the contact between the two suites. Thus, marl and marly limestones (Miocene) provide average resistivity values, in contrast to the low values of the clays from the upper section of the Triassic unit.

5. Conclusions

In this study, different geophysical methods were combined to analyse the capacity of each method in modelling geological structures with mining implications. For this purpose, the old mining district of Linares-La Carolina (southeast of Spain), where PbS ores have been exploited, was chosen. More specifically, the western sector of the mining district was studied, where mining was limited by the presence of fractures.

Three different geophysical techniques have been used: seismic reflection, electrical resistivity tomography (ERT) and time-domain electromagnetic (TDEM) methods. These geophysical techniques have been calibrated thanks to direct and available information, both from outcrop data and from mining research and groundwater boreholes. The seismic reflection profiles show abrupt changes in the wave amplitude associated with the sedimentary cover, as well as the acoustic basement associated with the Palaeozoic basement. Using this method, the fractures that displaces downward the eastern sector (Bailén Graben) are detected, even indicating different fracturing stages. However, the method has not made it possible to differentiate phyllites and granitoids in this Palaeozoic substrate.

TDEM is highly versatile and can be used with different configurations, amplitudes, voltages, time, device ranges and loop size, depending on the depth of study. In this study, the fit between the seismic and electromagnetic data was generally good. This method has made it possible to detect the depth of the Palaeozoic basement under the sedimentary cover, as well as different fractures.

At depths lower than 200 m, based on variations in the resistivity values, ERT profiles also identify the basement-sedimentary cover contact, as well as the different fractures. This technique even makes it possible to differentiate, within the basement, between the granite intrusion and the phyllites. This result has an evident mining importance because the metallised veins are associated with competent rocks (granitoids and metamorphic aureole), which quickly turn into waste rock when the host rock consists of phyllites.

The subsidence of the granite stock towards the east has been determined by the movement of a fault before the Triassic deposit, reducing the likelihood that well-metallised veins will be found in the Palaeozoic of the Bailén graben towards the east of this structure.

Declaration of Competing Interest

The authors declare that they have no known competing financial interests or personal relationships that could have appeared to influence the work reported in this paper.

Acknowledgements

Research has been supported by the University of Jaén. The authors thank two anonymous reviewers for their critical comments which significantly improved the manuscript.

References

André, F., van Leeuwen, C., Saussez, S., Van Durmen, R., Bogaert, P., Moghadas, D., de Rességuier, L., Delvaux, B., Vereecken, H., Lambot, S., 2012. High-resolution imaging of a vineyard in south of France using ground-penetrating radar, electromagnetic induction and electrical resistivity tomography. J. Appl. Geophys. 78, 113–122.

Auken, E., Jørgensen, F., Sørensen, K.I., 2003. Large-scale TEM investigation for groundwater. Explor. Geophys. 34 (3), 188–194.

Azcárate, J.E., 1977. Mapa geológico y memoria explicativa de la hoja 905 (Linares). escala 1:50.000. Instituto Geológico y Minero de España.

Binley, A., Hubbard, S.S., Huisman, J.A., Revil, A., Robinson, D.A., Singha, K., Slater, L. D., 2015. The emergence ofhydrogeophysics for improvedunderstanding of subsurface processesover multiple scales. Water Resour. Res. 51 (6), 3837–3866.

Christiansen, A.V., Auken, E., Sorensen, K., 2009. The transient electromagnetic method. In: Kirsch, R. (Ed.), Groundwater Geophysics, A Tool for Hydrogeology. Springer, pp. 179–224.

Dahlin, T., Zhou, B., 2004. A numerical comparison of 2D resistivity imaging with 10 electrode arrays. Geophys. Prospect. 52 (5), 379–398.

Danielsen, J.E., Auken, E., Jorgensen, F., Sondergaard, V., Sorensen, K., 2003. The application of the transient electromagnetic method in hydrogeophysical survey. J. Appl. Geophys. 53, 181–198.

Dennis, Z.R., Cull, J.P., 2012. Transient electromagnetic survey for the measurement of near-surface electrical anisotropy. J. Appl. Geophys. 76, 64–73.

ENADIMSA (unpublished). Investigación de la demarcación San Juan al Oeste de la Falla de Guarromán-Filón I. 1985.

Fitterman, D.V., Steward, M.T., 1986. Transient electromagnetic soundings for groundwater. Geophysics 51, 995–1006.

Goldman, M., Rabinovich, B., Rabinovich, M., Gilad, D., Gev, I., Schirov, M., 1994. Application of the integrated NMR-TDEM method in groundwater exploration in Israel. J. Appl. Geophys. 31 (1-4), 27–52.

Gómez-Ortiz, D., Fernández-Remolar, D.C., Granda, A., Quesada, C., Granda, T., Prieto-Ballesteros, O., Molina, A., Amils, R., 2014. Identification of the subsurface bodies responsible for acidity in Rio Tinto source water; Spain. Earth Planet. Sci. Lett. 391, 36–41.

Granda Sanz, Ángel, Granda París, Teresa, Pons, Juan Manuel, Videira, Juan Carlos, 2019. El descubrimiento del Yacimiento de la Magdalena. Protagonismo de los métodos geofísicos en la exploración de yacimientos tipo sulfuros masivos vulcanogénicos (vms) profundos en la faja pirítica ibérica. Boletín Geológico y Minero 130 (2), 213–230.

Hallbauer-Zadorozhnaya, V.Y., Stettler, E., 2009. Time Domain Electromagnetic Sounding to delineate hydrocarbon Contamination of ground water. Symposium on the Application of Geophysics to Engineering and Environmental Problems 2009, 241–251.

Hu, Y., Zeng, Z., Chen, X., Zhao, X., 2016. In: Application of Transient Electromagnetic Method in saturation region detection in tailings dam. Atlantis Press, pp. 318–321.

IGME (unpublished), 1983. Exploración Geológico-Minera de la fosa tectónica de Bailén (Jaén). Sismica de reflexión.

Kafria, Uri, Goldman, Mark, 2006. Are the lower subaquifers of the Mediterranean coastal aquifer of Israel blocked to seawater intrusion? Results of a TDEM (time domain electromagnetic) study. Israel J. Earth Sci. 55 (2), 55–68.

Larrea, F.J., Carracedo, M., Ortega Cuesta, L., Gil Ibarguchi, J.I., 1994. El Plutón de Linares (Jaén): cartografía, petrología y geoquímica. Cuaderno Lab. Xeológico de Laxe Coruña 19, 335–346.

Levi, E., Goldman, M., Hadad, A., Gvirtzman, H., 2008. Spatial delineation of groundwater salinity using deep time domain electromagnetic geophysical measurements: A feasibility study. Water Resour. Res. 44, W12404. https://doi.org/10.1029/2007WR006459.

Lillo, J., 1992. Geology and Geochemistry of Linares-La Carolina Pb-Ore field (Southeastern border of the Hesperian Massif). Ph. D. Thesis, Univ. Leeds.

Loke, M. H., 2014. Tutorial: 2-D and 3-D electrical imaging surveys, Revision date: 5th November 2014. www.geotomosoft.com.

Loke, M.H., Barker, R.D., 1996. Rapid least-squares inversion of apparent resistivity pseudosections by a quasi-Newton method. Geophys. Prospect. 44, 131–152.

Loke, M.H., Dahlin, T., 2002. A comparison of the Gauss-Newton and quasi-Newton methods in resistivity imaging inversion. J. Appl. Geophys. 49 (3), 149–162.

McNeill, J.D., 1994. Principles and application of time domain electromagnetic techniques for resistivity sounding. Technical Note TN-27, Geonics Ltd, Ontario. http://www.geonics.com/pdfs/technicalnotes/tn27.pdf.

Maillet, Grégoire M., Rizzo, Enzo, Revil, André, Vella, Claude, 2005. High resolution electrical resistivity tomography (ERT) in a transition zone environment: Application for detailed internal architecture and infilling processes study of a Rhône River paleo-channel. Mar. Geophys. Res. 26 (2-4), 317–328.

Martínez, J., Benavente, J., García-Aróstegui, J.L., Hidalgo, M.C., Rey, J., 2009. Contribution of electrical resistivity tomography to the study of detrital aquifers affected by seawater intrusión-extrusion effects: the river Vélez delta (Vélez-Málaga, southern Spain). Eng. Geol. 108, 161–168.

Martínez, J., Hidalgo, M.C., Rey, J., Garrido, J., Kohfahl, C., Benavente, J., Rojas, D., 2016. A Multidisciplinary Characterization of a Tailings Pond in the Linares-La Carolina Mining District, Spain. J. Geochem. Explor. 162, 62–71.

Martínez, J., Rey, J., Sandoval, S., Hidalgo, M.C., Mendoza, R., 2019. Geophysical prospection using ERI and IP techniques to locate vein deposits. Remote Sens. 11 https://doi.org/10.3390/rs11242923.

Martínez-Pagán, Pedro, Faz Cano, Ángel, Aracil, Enrique, Arocena, Joselito M., 2009. Electrical resistivity imaging revealed the spatial properties of mine tailing ponds in the Sierra Minera of Southeast Spain. J. Environ. Eng. Geophys. 14 (2), 63–76.

Martínez-Segura, Marcos A., Vásconez-Maza, Marco D., García-Nieto, María C., 2020. Volumetric characterisation of waste deposits generated during the production of fertiliser derived from phosphoric rock by using LiDAR and electrical resistivity tomography. Sci. Total Environ. 716, 137076. https://doi.org/10.1016/j.scitotenv.2020.137076.

Nabighian, N.M., 1988. Electromagnetic method in Applied Geophysics. Society of Exploration Geophysics, Tulsa, Okla, p. 971.

Perconing, E., 1971. Sobre la edad de la Transgresión del Terciario marino en el borde meridional de la Meseta. *Congr. Hispano-Luso-Americano de Geología Económica.* Madrid. Sección 1, 309–319.

Rey, J., Martínez, J., Hidalgo, M.C., 2013a. Investigating fluvial features with electrical resistivity imaging and ground-penetrating radar: The Guadalquivir River terrace (Jaen, Southern Spain). Sed. Geol. 295, 27–37.

Rey, J., Martínez, J., Hidalgo, M.C., Rojas, D., 2013b. Heavy metal pollution in the Quaternary Garza basin: a multidisciplinary study of the environmental risks posed by mining (Linares, southern Spain). Catena 110, 234–242.

Rey, J., Martínez, J., Mendoza, R., Sandoval, S., Tarasov, V., Kaminsky, K., Hidalgo, M.C., Morales, K., 2020. Geophysical characterization of aquifers in southeast Spain using ERT, TDEM, and vertical seismic reflection). Appl. Sci. 10, 7365. https://doi.org/10.3390/app10207365.

Rey, J., Martínez, J., Hidalgo, M.C., Mendoza, R., Sandoval, S., 2021. Assessment of tailings ponds by a combination of electrical (ERT and IP) and hydrochemical techniques (Linares, southern Spain)Bewertung von Absetzteichen durch eine Kombination von elektrischen (ERT und IP) und hydrochemischen Methoden (Linares, Südspanien)Evaluación de los diques de colas mediante una combinación de técnicas eléctricas (ERT e IP) e hidroquímicas (Linares, sur de España)电法(ERT和IP)与水化学联合方法的尾矿库评价(西班牙南部利纳勒斯). Mine Water Environ. 40 (1), 298–307. https://doi.org/10.1007/s10230-020-00709-3.

Sasaki, Y., 1992. Resolution of resistivity tomography inferred from numerical simulation. Geophys. Prospect. 40, 453–464.

Sridhar, M., Markandeyulu, A., Chaturvedi, A.K., 2017. Mapping subtrappean sediments and delineating structure with the aid of heliborne time domain electromagnetics: Case study from Kaladgi Basin, Karnataka. J. Appl. Geophys. 136, 9–18.

Store, H., Storz, W., Jacobs, F., 2000. Electrical resistivity tomography to investigate geological structures of earth's upper crust. Geophys. Prospect. 48, 455–471.

Telford, W.M., Geldart, L.P., Sheriff, R.E., 1990. Applied Geophysics. Cambridge University Press, p. 770.

Xue, Guo-Qiang, Qin, Ke-Zhang, Li, Xiu, Li, Guang-Ming, Qi, Zhi-Peng, Zhou, Nan-Nan, 2012. Discovery of a Large-scale Porphyry Molybdenum Deposit in Tibet through a Modified TEM Exploration Method. J. Environ. Eng. Geophys. 17 (1), 19–25.